Molecular Biology of the Cell
Vol. 17, 5275–5286, December 2006

Enlazin, a Natural Fusion of Two Classes of Canonical Cytoskeletal Proteins, Contributes to Cytokinesis Dynamics[V]

Edelyn Octtaviani, Janet C. Effler, and Douglas N. Robinson

Department of Cell Biology, Johns Hopkins School of Medicine, Baltimore, MD 21205

Submitted August 30, 2006; Revised September 28, 2006; Accepted October 5, 2006
Monitoring Editor: Yu-li Wang

Cytokinesis requires a complex network of equatorial and global proteins to regulate cell shape changes. Here, using interaction genetics, we report the first characterization of a novel protein, enlazin. Enlazin is a natural fusion of two canonical classes of actin-associated proteins, the ezrin-radixin-moesin family and fimbrin, and it is localized to actin-rich structures. A fragment of enlazin, enl-tr, was isolated as a genetic suppressor of the cytokinesis defect of *cortexillin-I* mutants. Expression of enl-tr disrupts expression of endogenous enlazin, indicating that enl-tr functions as a dominant-negative lesion. Enlazin is distributed globally during cytokinesis and is required for cortical tension and cell adhesion. Consistent with a role in cell mechanics, inhibition of *enlazin* in a *cortexillin-I* background restores cytokinesis furrowing dynamics and suppresses the growth-in-suspension defect. However, as expected for a role in cell adhesion, inhibiting *enlazin* in a *myosin-II* background induces a synthetic cytokinesis phenotype, frequently arresting furrow ingression at the dumbbell shape and/or causing recession of the furrow. Thus, enlazin has roles in cell mechanics and adhesion, and these roles seem to be differentially significant for cytokinesis, depending on the genetic background.

INTRODUCTION

Cell shape changes are critical for a variety of biological processes, including neuronal extension, formation of a columnar epithelium, cell motility, and cytokinesis. Cytokinesis, the mechanical separation of a mother cell into two daughter cells, is essential for cell health. Failure of this important process can lead to defects in cell growth and aneuploidy, causing diseases such as cancer (Daniels *et al*., 2004; Dey, 2004; Stukenberg, 2004; Fujiwara *et al*., 2005).

Cytokinesis is coordinated by the mitotic spindle, which delivers spatiotemporal cues to the actin-rich cortex, leading to a redistribution of a number of cytoskeletal proteins, including myosin-II, to the equator of the cell (Rappaport, 1996). Classic models of cytokinesis assign myosin-II the role of major radial force-producer that constricts the equatorial actin ring, producing two daughter cells (De Lozanne and Spudich, 1987; Zurek *et al*., 1990; He and Dembo, 1997; Zang *et al*., 1997; Robinson *et al*., 2002a). Puzzlingly, cytokinesis in some cell types proceeds fairly normally without myosin-II, suggesting that cells have multiple mechanisms for driving furrow ingression (Kanada *et al*., 2005). Other observations suggest that both the polar/global and equatorial regions of the cell cortex have important roles in the contractile process (Robinson and Spudich, 2000; Matzke *et al*., 2001; O'Connell *et al*., 2001; Kurz *et al*., 2002; Nagasaki *et al*., 2002).

This article was published online ahead of print in *MBC in Press* (http://www.molbiolcell.org/cgi/doi/10.1091/mbc.E06–08–0767) on October 18, 2006.

[V] The online version of this article contains supplemental material at *MBC Online* (http://www.molbiolcell.org).

Address correspondence to: Douglas N. Robinson (dnr@jhmi.edu).

Abbreviations used: CH, calponin homology; ERM, ezrin-radixin-moesin; FERM, Band 4.1-ezrin-radixin-moesin.

To establish quantitatively the roles of equatorial and global pathways in cytokinesis mechanics, we recently demonstrated that both radial stresses at the cleavage furrow cortex and resistive stresses at the global polar cortex help control cytokinesis dynamics (Zhang and Robinson, 2005). In particular, contractility is driven by actively generated radial stresses from equatorial myosin-II and cortexillin-I and what is probably an intrinsic Laplace pressure due to stresses in the viscoelastic cytoskeletal network, whereas the resistive stresses are established by globally distributed proteins such as dynacortin and RacE small GTPase. Thus, cytokinesis seems to be executed by a complex network, involving multiple force-generating systems. Consequently, many proteins may contribute important functions to cytokinesis without producing gross phenotypes when mutated (Eggert *et al*., 2004; Skop *et al*., 2004). However, at present we still know very little about how the cytokinesis machinery works.

To probe the biocomplexity of cytokinesis, we used interaction genetics in the protozoan *Dictyostelium discoideum*. In particular, we used genetic suppression approaches to identify molecules whose loss-of-function phenotypes may be mild but that become more apparent in the context of other mutations. Using this approach, genes are functionally selected rather than isolated by screening thousands of clones for subtle phenotypes. Previously, we identified a version of dynacortin as a genetic suppressor of mutants of the equatorially localized actin cross-linker cortexillin-I (Robinson and Spudich, 2000). Significantly, inhibition of dynacortin produces a mild morphological phenotype, but on more quantitative inspection, it has significant roles in cell mechanics and in controlling cytokinesis dynamics (Girard *et al*., 2004; Zhang and Robinson, 2005; Girard *et al*., 2006). Thus, identification of relevant genes by using morphological criteria alone is insufficient for identifying the molecular bases of robust, dynamic, and complex processes such as

cytokinesis, but rather it requires sophisticated genetic approaches.

In this article, we present the characterization of a novel protein, that we named enlazin, a fragment of which was identified in our original *cortexillin-I* suppressor screen (Robinson and Spudich, 2000). Enlazin is a natural fusion of two classes of familiar actin cytoskeletal proteins, the ezrin-radixin-moesin (ERM)-family of membrane–actin-tethering proteins and the actin cross-linker fimbrin. A truncated version of enlazin suppresses the growth-in-suspension defects of *cortexillin-I* mutants and disrupts endogenous enlazin expression. We demonstrate that enlazin contributes to cell adhesion and cortical mechanics. From these data, we propose that enlazin contributes to the resistance generated by the global cortex and to force generation through adhesion to the substrate, both of which contribute to cytokinesis dynamics.

MATERIALS AND METHODS

Dictyostelium Strains and Cell Culture

Parental "wild-type" strains include Ax3:Rep orf+ cells (Robinson and Spudich, 2000), Ax2 cells, and *myoII*$^-$::GFPmyoII:pDRH-Hyg^R, RFPα-tubulin:pDxA-Bl^R cells. The *myosin II* null cell line (*myo II*$^-$) was the HS1 (*mhcA*$^-$) strain (Ruppel *et al*., 1994). The *cortI*^{1151} cells (HS1151) have been described previously (Robinson and Spudich, 2000). The Δ*cortI* strain is a deletion of the *cortexillin-I* locus generated by homologous recombination in the wild-type Ax2 background (Faix *et al*., 1996).

Ax3:Rep orf+ strains were grown in Hans' enriched HL-5 media (1.4X HL-5 and 8% FM) plus 60 U/ml penicillin, 60 μg/ml streptomycin sulfate, and plus or minus 15–30 μg/ml Geneticin (G-418), depending on whether the cells were transformed with an episomal plasmid. Ax2–214 and *myoII* strains with episomal plasmids were grown in 10–20 μg/ml G-418 or 5–15 μg/ml hygromycin, as appropriate. *myoII*$^-$::GFPmyoII:pDRH-Hyg^R, RFPα-tubulin:pDxA-Bl^R derivatives were grown in 2 μg/ml blasticidin, 2.5 μg/ml hygromycin, and 30 μg/ml G-418 after transformation with pLD1A15SN-based vectors. Cells were propagated at 22°C on 10-cm plates. For suspension growth assays, cells were grown in 10-ml culture volumes in 125-ml Erlenmeyer flasks at 200 rpm. Cell densities were determined using a hemacytometer. Plasmids were transformed into *Dictyostelium* as described previously (Robinson and Spudich, 2000).

Dictyostelium Expression Plasmids

The expression vectors used were pLD1A15SN, pDxA-Bl, or a Ddp1-based hygromycin-resistant plasmid pDRH-Hyg^R (Robinson and Spudich, 2000; Effler *et al*., 2006). All plasmids have been engineered to have identical polylinkers. All cDNA fragments (including untagged genes, green fluorescent protein [GFP] or red fluorescent protein [RFP]-fusions, and hairpin constructs) were generated to have SalI and NotI ends or SalI and MluI ends, allowing the gene fragments to be moved from vector to vector without redesign.

Enl-tr construct encodes amino acid residues 92-497 and was isolated by selection as a suppressor of *cortI*^{1151} cells (Robinson and Spudich, 2000). *Enlazin* full-length constructs with (enlfl; including all amino acid residues 1-1503) and without (enlfl-N; including amino acid residues 1-1462) the carboxyl terminal poly-N tail were generated by polymerase chain reaction (PCR) amplification from genomic DNA and was assembled and verified by DNA sequence analysis. These constructs were assembled in pLD1A15SN. The *enlazin* hairpin construct (enlhp) was generated by cloning bases 1-1483 in the antisense orientation in SalI and NotI sites of pLD1A15SN; this generated the construct enlAS:pLD1. The sense fragment spanning bases 857-1462 was ligated into the NotI and MluI sites of enlAS:pLD1, generating enlhp:pLD1. GFP-enlfl was assembled by adding 5′ XbaI site and a 3′ NotI site (added after the translation terminator) to the *enlazin* full-length cDNA by using PCR and subcloning into a GFPS65T tagging vector (GFP2:pBS), by using the XbaI site and NotI sites. GFP-enl was subcloned into pLD1A15SN and pDRH-Hyg^R as a SalI-NotI fragment. To examine interactions with Δ*cortI-214*, which has *cortexillin-I* deleted using a G418^R marker (Faix *et al*., 1996), enl-tr:pDRH-Hyg^R and GFP-cortexillin-I:pDRH-Hyg^R were constructed by moving the respective cDNAs from pLD1A15SN to pDRH-Hyg^R as SalI–NotI fragments. GFP-α-tubulin and RFP-α-tubulin were also constructed in pDRH-Hyg^R or pDxA-Bl^R as a SalI–NotI fragment.

Growth Rate and Nuclei/Cell Ratio Determination

Relative growth rates were determined by diluting the cells to a similar starting density and measuring the cell densities over several subsequent time points with a hemacytometer. The cell densities were plotted versus time and the resulting log phase curve was fit to a single exponential equation by using KaleidaGraph (Synergy Software, Reading, PA). The wild-type control strain was normalized to 1, and growth rates of other strains within each growth experiment were normalized to the wild-type control. The relative growth rates for each strain were averaged, and the SEM was determined. Statistical significance was determined using a two-tailed Student's *t* test.

During the log phase of growth, aliquots of cells were removed and fixed with −10°C methanol for 2 min. Cells were washed three times in PBT (1X phosphate-buffered saline, 0.5% bovine serum albumin [BSA], and 0.05% Triton X-100). Cells were stained with 1 μg/ml 4,6-diamidino-2-phenylindole (Invitrogen, Carlsbad, CA) for 20 min with gentle rocking. After washing, the cells were examined by fluorescence microscopy using an IX81 microscope (Olympus American, Melville, NY).

RNA Analysis

Total RNA was isolated using the TRIzol method (Invitrogen). RNA was quantified using a SmartSpec spectrophotometer (Bio-Rad, Hercules, CA), separated on a 1% agarose-formaldehyde gel and transferred to Hybond-N$^+$ nylon membrane (GE Healthcare, Little Chalfont, Buckinghamshire, United Kingdom) by capillary transfer. The *fimbrin* domain (nucleotides 2857-4380) of *enlazin* was labeled using the random hexamer labeling (Feinberg and Vogelstein, 1983). Immobilized RNAs were hybridized with denatured α-^{32}P-labeled DNA probes in Church's buffer (250 mM sodium phosphate, pH 7.0, 7% SDS, 1% BSA, and 1 mM EDTA). Hybridized RNAs were detected using an FX PhosphorImager (Bio-Rad).

Antibody Production and Western Analysis

The *enlazin* bases 2140-2855 (encoding amino acids 714-952; intervening region [IVR] region of enlazin) was expressed in *Escherichia coli* as a His-tagged protein by using pET14b vector (Novagen, Madison, WI). His-IVR protein was purified on Ni^{2+} Superflow resin (GE Healthcare), by using standard conditions. Rabbit polyclonal antibodies were generated using a standard protocol for antibody production.

For Western analysis, cell lysates were prepared by boiling cells in SDS sample buffer, electrophoretically separated on SDS-polyacrylamide gels, and transferred to nitrocellulose. Enlazin protein was detected using the anti-enlazin IVR rabbit polyclonal antibody and a goat anti-rabbit, horseradish peroxidase-conjugated, 2° antibody (Bio-Rad). Immune complexes were detected using the ECL detection system (GE Healthcare) and a VersaDoc imaging station (Bio-Rad).

Immunocytochemistry

For in situ localization of the endogenous enlazin, cells were plated on coverslips and allowed to adhere for 4 h to overnight. Cells were fixed for 5 min in fixation buffer (4% paraformaldehyde [Electron Microscopy Sciences, Ft. Washington, PA], 150 mM NaCl, and 0.1% Triton X-100). Cells were blocked for 10 min in PBT. Cells were immunostained with the anti-enlazin polyclonal antibodies (1:1000) in PBT. Antibodies were detected by indirect immunofluorescence using fluorescein isothiocyanate-conjugated donkey anti-rabbit secondary antibodies (Invitrogen) as appropriate. All washes were done in PBT.

Cell Imaging

For fixed and live cells, differential interference contrast (DIC) and epifluorescence imaging was done with a 40× (numerical aperture [NA] 1.3) objective and a 1.6× Optivar. A 60× (NA 1.45) objective with a 1.6× Optivar was used for three-dimensional (3D)-deconvolution and total internal reflection fluorescence (TIRF) imaging. For 3D-deconvolution, images were collected using 0.38-μm steps and deconvolved using a measured point spread function and the MetaMorph 3D-deconvolution module. A xenon lamp was used for illumination for wide-field epifluorescence and 3D-deconvolution imaging, and a 488-nm laser was used for TIRF imaging. All images were collected using an IX81 microscope equipped with the MetaMorph Software package (Molecular Devices, Sunnyvale, CA) and processed with Adobe Photoshop (Adobe Systems, Mountain View, CA). All live-cell imaging was performed at 22 ± 1°C.

For cytokinesis dynamics analysis, DIC movies were collected with 2-s time resolution, and cells were analyzed as described previously (Zhang and Robinson, 2005). In this method, the minimal furrow diameter and furrow length at 4-s time resolution were measured. The time-point when the length and diameter were equal (the crossover distance, D_x) was defined as the crossover time (T_x). T_x was set to time 0, and the diameters were rescaled by dividing each diameter by D_x. Thus, all curves pass through the point (0,1), which is where T_x and D_x were found. The mean ± SEM D_x for each strain is presented on the graphs (Figure 6).

Cell Adhesion Assay

Log-phase cells were seeded in 2 ml of Hans' enriched HL-5 media in six-well plates. Both tissue-culture–treated and nontreated plates were used with similar results. Cells were incubated for 4 h (initial seeding density of 1×10^6 cells/ml) or overnight (initial seeding density of 3×10^5 cells/ml) at 22°C

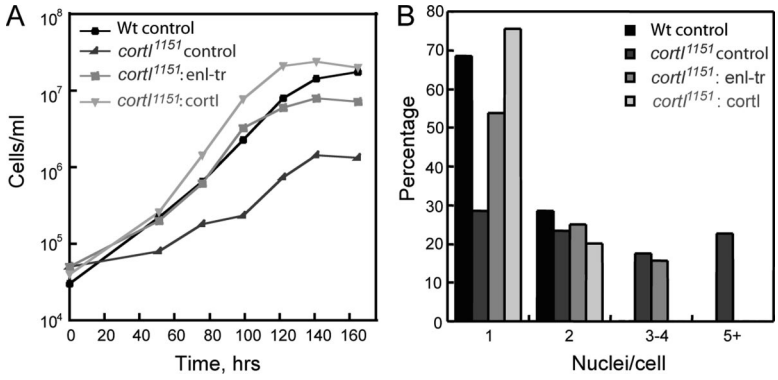

Figure 1. Enl-tr suppresses the growth-in-suspension defect of *cortI*^{1151} cells. (A) Representative growth curve showing the change in cell density as a function of time for wild-type control, *cortI*^{1151} control, *cortI*^{1151}:enl-tr, and *cortI*^{1151}:cortI cells. Control cells carry the empty pLD1A15SN vector, the backbone vector for the enl-tr and cortI constructs. (B) Distribution of nuclei/cell from the same strains as in A. Approximately 300 cells were counted for each genotype.

without agitation. Specific conditions for each experiment are noted in the figure legends. Samples were then rotated at a specified speed (rpm) for 1 h. Detached cell density and the total cell density were measured. Typically, three to five samples were counted at each rpm for each genotype.

Micropipette Aspiration

Our motorized micropipette aspiration setup was presented previously (Effler *et al*., 2006). In short, borosilicate capillaries (o.d., 1.0 mm, i.d. 0.75 mm, 10 cm; Sutter Instrument, Novato, CA) were pulled to an inner diameter of 6 μm (PMP102 micropipette puller; MicroData Instruments, Woodhaven, NY) and filled with sterile filtered 1X phosphate-buffered saline. During the loading process, the needle, tubing, and pipette chambers were examined to ensure that air bubbles were not present within the system. Log-phase cells were transferred to imaging chambers and allowed to settle for 15 min, and all measurements were made with the cells cultured in Hans' enriched HL-5 media at 22°C. Cells were aspirated until the equilibrium length of the cortex tether pulled into the pipette (L_p) was equal to the radius of the pipette (R_p), forming a hemispherical deformation. The cell radius (R_c) was also measured. The aspiration pressure (ΔP) was calculated, using the hydrostatic equation $\Delta P = \rho gh$, where g is the gravitational constant (9.8 m/s^2), h is the differential height between the reference tank and the movable tank, and ρ is the density of water (1000 kg/m^3). This pressure was then converted to nanonewtons per square micrometer. The effective cortical tension (T) was calculated from the Law of Laplace ($T = \Delta P/(2(1/R_p - 1/R_c))$ (Evans and Yeung, 1989; Derganc *et al*., 2000). By applying pressure to reach a hemispherical deformation ($L_p = R_p$), we measure an effective cortical tension of a specific geometric shape for each strain, removing ambiguity associated with determining a specific critical pressure for active, healthy cells (Derganc *et al*., 2000).

RESULTS

Enl-tr Suppresses Cortexillin-I Mutants

Previously, we conducted a genetic suppression analysis of *cortexillin-I* mutant cells (Robinson and Spudich, 2000). From this, we isolated a plasmid clone (2B25), which encoded a fragment (enl-tr) of a 1503-amino acid protein that we named enlazin (Figures 1 and 2). Because the original report focused on dynacortin (Robinson and Spudich, 2000), we begin here with the essential recapitulation of the enl-tr suppression of *cortexillin-I* mutant cells, which has a suspension-growth defect. On reintroduction, enl-tr increased the growth rate in suspension culture of *cortI*^{1151} cells (Figure 1A and Table 1). The *cortI*^{1151} cells show a broader distribution of number of nuclei per cell, indicating a cytokinesis defect, whereas the distribution for *cortI*^{1151}:enl-tr cells was significantly shifted toward a more wild-type distribution (Figure 1B). Rescue of *cortI*^{1151} by cortexillin-I is shown for comparison.

We also verified that suppression of *cortexillin-I* by enl-tr was not genetic background specific by testing its ability to suppress a second *cortexillin-I* mutant, Δ*cortI-214* (Faix *et al*., 1996). Indeed, enl-tr partially rescued the growth in suspension defect of this mutant, demonstrating that enl-tr suppresses the *cortexillin-I* requirement in these different genetic backgrounds (Table 1).

Enlazin Is a Fusion of Two Classes of Cytoskeletal Proteins

Full-length enlazin is a large, multidomain protein that includes an amino-terminal talin-like domain, an α-helical domain, and a fimbrin domain (Figure 2A). The genome project named the *enlazin* locus *fimB* due to its fimbrin domain (dictybase.org). Because of the multidomain structure, we suggest that this gene product represents a novel class of proteins, rather than a simple fimbrin-family member, although homologues in other organisms have yet to be identified. Thus, we have named the protein enlazin, from the Spanish *enlazar*, which means "to connect."

The amino-terminal ~300 amino acids seem to define a Band 4.1-ezrin-radixin-moesin (FERM)-like domain (Figure 2B). Blast searches and pairwise alignments reveal that residues 8–139 are most similar (27% identical and 49% similar) to the amino-terminal 122 amino acids of talin (including the first approximately one-third of the FERM domain of talin). Residues from ~194–390 are 27% identical and 48% similar to *Dictyostelium* protein kinase 5 with the strongest region of similarity spanning residues 210–290, which is identified as a plekstrin homology (PH) domain (Figure 2C). The FERM domain has a tripartite structure with the third part having structural similarity to PH domains and corresponds in the linear sequence approximately to the PH domain-related region of enlazin (Figure 2B). Given the presence of the talin-homology region and the PH domain, the amino-terminal 300-amino acid region of enlazin resembles a FERM-like domain.

The FERM-like domain of enlazin is followed by an ~400-amino acid α-helical domain that has a high probability for forming a coiled coil (Figure 2D). This α-helical region is 25% identical and 46% similar to the α-helical region of radixin. The combination of a FERM-like domain and α-helical region is strongly reminiscent of ERM proteins. However, instead of the short actin-binding domain found at the carboxy terminus in ERMs, enlazin has a 240-amino acid stretch that has no apparent homology to other proteins. We refer to this region as the IVR. The final 550 amino acids of enlazin are most similar (28% identical and 49% similar) to *Oryza sativa* fimbrin (Figure 2E). The enlazin fimbrin domain is 26% identical and 45% similar to mammalian T-plastin across the four T-plastin calponin homology (CH) domains. However, domain prediction algorithms only clearly identify three CH domains in enlazin. Furthermore, from pairwise and multisequence alignments, the similarity to other fimbrins is reduced in the fourth CH domain, although the protein is long enough for a distantly related CH domain to be present. Thus, it is unclear whether the fimbrin domain of enlazin will form two complete actin-binding domains, be-

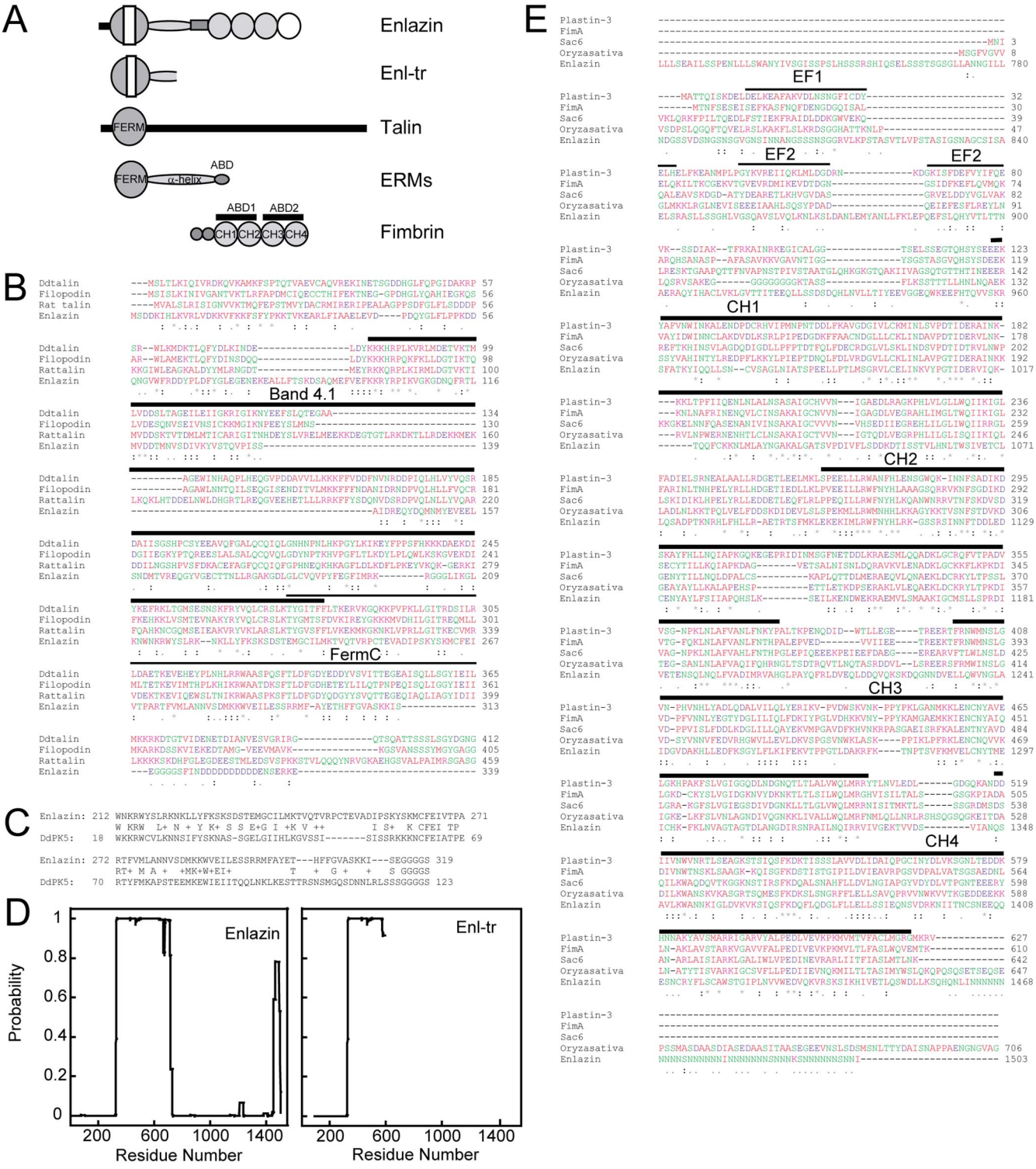

Figure 2. Enlazin protein is related to two classes of cytoskeletal proteins. (A) Cartoon depicting the domain structure of enlazin as it compares to talin, ERMs, and fimbrin. Enl-tr encodes a portion of the FERM and α-helical domains and was identified as a suppressor of *cortexillin-I* mutants. (B) ClustalW multisequence alignment of the amino terminal region of enlazin compared with two *Dictyostelium* talin-family proteins (Ddtalin and filopodin) and rat talin. The Band4.1 and FermC regions are identified. (C) Pairwise alignment between the FermC region of enlazin and the closest PH-domain of *Dictyostelium* protein kinase 5 (DdPK5). (D) Coils analysis of enlazin and enl-tr. The α-helical region scores a high probability to form coiled coils by this algorithm. (E) ClustalW multisequence alignment of fimbrin homology region of enlazin with mammalian plastin-3, *Dictyostelium* fimA, yeast sac6, and *Oryza sativa* fimbrin. The EF-hands (EF1 and EF2) and the four CH domains are identified. Enlazin seems to be highly diverged in the EF-hands and CH4 domain.

Table 1. Growth rate data for *enlazin* mutants

Strain	Relative *k* (mean ± SEM)	n
Wt control[a]	[1]	17
Wt:enl-tr	1.1 ± 0.05	15
cortI^{1151} control[a]	0.55 ± 0.05	10
cortI^{1151}:enl-tr	0.78 ± 0.04	11
cortI^{1151}:cortI	1.1 ± 0.06	9
Wt:enlhp	0.66 ± 0.06	4
cortI^{1151}:enlhp	0.42 ± 0.03	4
Δ*cortI-214*:cortI	[1]	6
Δ*cortI-214* control[a]	0.29 ± 0.03	6
Δ*cortI-214*:enl-tr	0.54 ± 0.03	6

[a] Control strains contain the empty vector.

cause each actin-binding domain is formed from two sequential CH domains.

Enlazin Is a Cortically Enriched Protein

After several unsuccessful attempts to recover an *enlazin*-deletion strain by using different knockout constructs, we silenced its expression using a hairpin construct (enlhp; Figure 3A). Silencing of genes by using hairpin constructs allows loss-of-function phenotypes to be studied with the added benefits that only the freshest phenotypes are analyzed and synthetic phenotypes with other deletion strains can be rapidly assessed (Girard *et al*., 2004; Zhang and Robinson, 2005; Girard *et al*., 2006). The ability to acquire fresh mutants rapidly is extremely valuable, because many deletion strains have phenotypes that are more severe immediately after they were generated, but then these strains adapt to the mutation over a few weeks of culture. To assess the phenotypes of enlazin, we generated transformants, verified expression inhibition, and analyzed the phenotypes within 2–3 wk of transformation for every experiment.

The enlhp construct was generated using the region of the *enlazin* cDNA that encodes the FERM domain. We verified that *enlazin* was silenced by Northern analysis using a probe to the fimbrin domain (Figure 3, B and C). We also generated anti-enlazin polyclonal sera by using the enl IVR as the antigen. Western analysis of wt:enlhp cells showed that no enlazin protein was detectable (Figure 3D). To help verify the enlazin band, we overexpressed enlazin from an episomal plasmid in wild-type cells (wt:enlOE; Figure 3D). Although enlazin is significantly overexpressed, we did not detect an obvious morphological or growth phenotype from the overexpression.

We then used the anti-enlazin antibodies to detect endogenous enlazin by immunocytochemistry (Figure 3E). Enlazin protein was distributed in the cortex and was enriched in cell surface protrusions. This cortical distribution was specifically due to enlazin, because all staining was absent in wt:enlhp cells and increased in wt:enlOE cells. The distribution is strongly reminiscent of several cytoskeletal proteins, including dynacortin, coronin, and actin (de Hostos *et al*., 1993; Robinson and Spudich, 2000). Live cell imaging of wild-type cells expressing GFP-enlazin fusion protein showed a similar cortical enrichment (Figure 3F and Supplemental Movie 1).

Because enlazin was discovered in the same genetic suppressor selection as dynacortin, we speculated that enlazin might assemble into punctate surface structures, which are probably the *Dictyostelium* equivalents of focal adhesions (Robinson *et al*., 2002b). To test this, we examined wt:GFP-enlazin cells by TIRF microscopy. Indeed, enlazin enriched in cell surface complexes similar to dynacortin and coronin (Figure 3G and Supplemental Movie 2). During cytokinesis, GFP-enlazin was distributed globally in the cytoplasm and cortex with enrichment in the membrane ruffles in wild-type and *myoII* mutant cells (Figure 3, H and I, and Supplemental Movies 3 and 4). This distribution was also observed for endogenous enlazin, which was detected using immunocytochemistry (data not shown). Similar to previous observations with dynacortin, enlazin becomes more cytoplasmic during early stages of cytokinesis when compared with interphase (Robinson and Spudich, 2000; Girard *et al*., 2004).

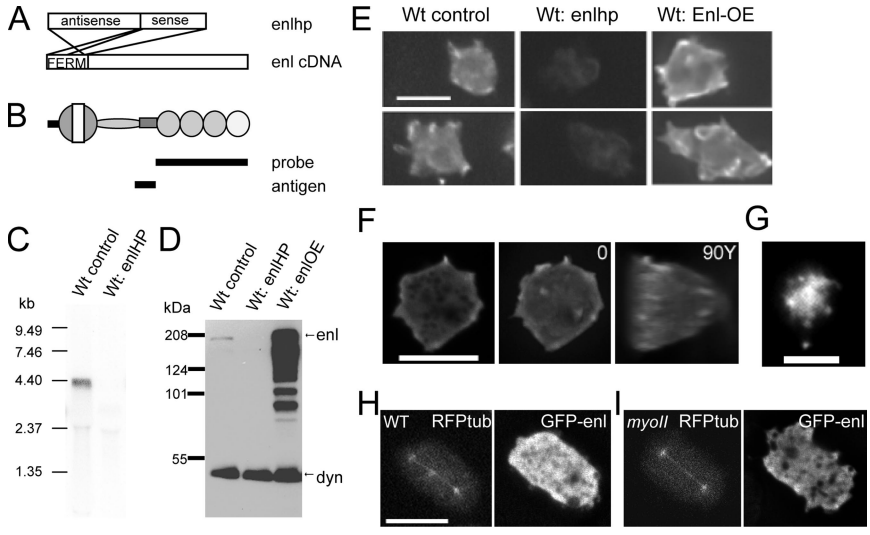

Figure 3. Silencing of *enlazin* by using RNA interference and enlazin is a cortex-enriched protein. (A) The enlhp hairpin construct was derived from sequences encoding the FERM domain. (B) The cDNA encoding the fimbrin domain of enlazin was used as the probe for Northern analysis. The IVR region was expressed, purified, and used as an antigen to raise anti-enlazin polyclonal antiserum. (C) Northern analysis reveals that there is no detectable transcript in cells expressing enlhp. (D) Western analysis also reveals that there is no detectable protein. Anti-dynacortin antiserum was also used to identify dynacortin as a loading control. (E) Anti-enlazin immunocytochemistry of wild-type control (empty vector), wt:enlhp, and wt:enl-OE (enlazin-overexpressing) cells shows that enlazin is enriched in the cortex, particularly in cell surface protrusions. Only low background fluorescence is detected in the wt:enlhp cells. (F) 3D-deconvolution of wild-type cells expressing GFP-enlazin demonstrates that enlazin is enriched in the cell cortex. Left, single optical section. Middle, 3D-reconstructed image. Right, 3D reconstructed image rotated 90° about the *y*-axis. (G) GFP-enlazin is enriched in cell surface adhesions as detected by TIRF imaging. (H and I) During cytokinesis, GFP-enlazin is distributed globally around the cortex in wild-type (H) and *myoII* mutant (I) cells. RFP-α-tubulin is shown, verifying that the cells are mitotic. Bars, 10 μm.

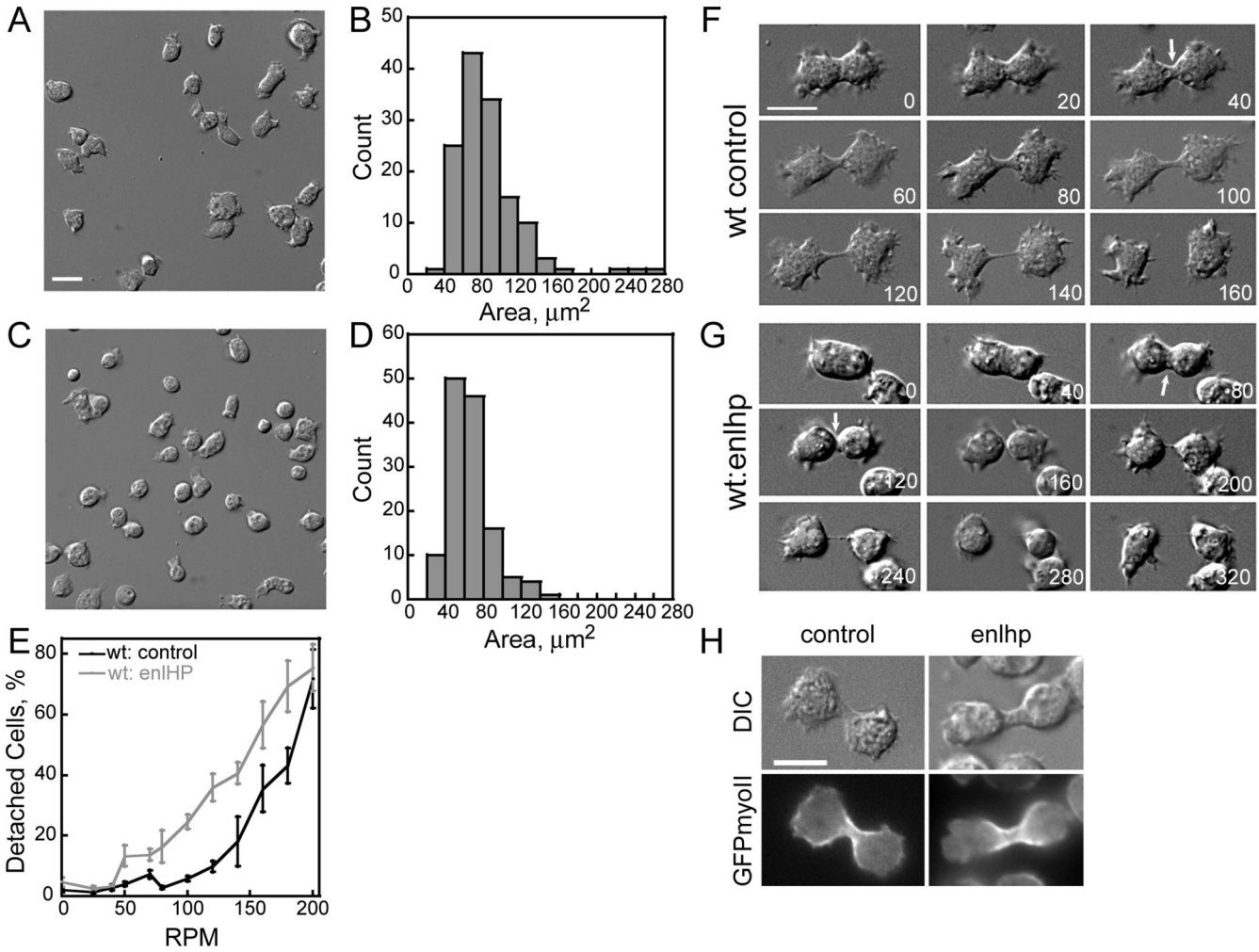

Figure 4. Enlazin is required for cell adhesion and cell morphology during cytokinesis. (A) DIC image of a field of wild-type control cells. (B) Distribution of cell area of wild-type control cells. (C) DIC image of a field of wt:enlhp cells. (C) Distribution of cell areas of wt:enlhp cells. (E) Adhesion assay of wt control and wt:enlhp cells. Cells were seeded at 1×10^6 cells/ml for 4 h on tissue-culture-treated six-well plates. After incubation, samples of cells were rotated at different rpm for an hour. Fraction of detached cells was then measured. Mean ± SEM of three to four replicas at each speed are plotted as a function of rpm. (F) DIC time series of a wild-type control cell undergoing cytokinesis. Wild-type cells establish an intercellular bridge (arrow) that continues to thin as the cell completes cytokinesis. (G) DIC time series of a wt:enlhp cell undergoing cytokinesis. Cylindrically shaped furrow begins to form at 80 s (arrow) but by 120 s, it collapses (arrow), probably due to a lack of adhesion by the cell. (F and G) Time 0 is start of the movie. Time, seconds. (H) GFPmyosin-II localizes normally to the cleavage furrow cortex in the absence of enlazin. The *wild-type* strain is a complemented *myosin-II* null:*myoII*:RFP-α-tubulin pDxA-Bl^R; GFP-myosin-II, pDRH-Hyg^R. Control cell in panel on left also contains the empty pLD1A15SN vector, whereas cell in panel on right contains the enlhp:pLD1 vector and expresses no enlazin. Bars, 10 μm. Bar in A also applies to C, and bar in F also applies to G.

Enlazin Contributes to Cell Growth and Adhesion

On transformation, wt:enlhp cells were slow to grow and populate a plate. To quantify this, we analyzed the growth rates of the cells in suspension culture. From initial rounds of growth in suspension, wild-type and *cortI*^{1151} cells expressing enlhp grew more slowly than the parental counterparts (Table 1). However, we noticed that after many rounds (>4) the growth rates of wt:enlhp and *cortI*^{1151}:enlhp cells approached the parental counterpart. From Western analysis, the increase in growth rate correlated with return of enlazin protein expression (data not shown). Thus, the slow growth rate corresponds to inhibition of *enlazin* by RNA interference.

During our analysis, we observed that wt:enlhp cells (area = 65 ± 1.9 μm^2; n = 132) seemed to be smaller than wild-type control cells (area = 86 ± 3.0 μm^2; n = 135; Student's two-tailed *t* test, $p < 0.0001$) but looked morphologically normal during interphase (Figure 4, A–D). Because a smaller area could be due to reduced cell size or reduced cell spreading, we examined cell size by using forward scatter by fluorescence-activated cell sorting (FACS) analysis. Wt control and wt:enlhp cells had an identical size distribution by FACS analysis (data not shown), indicating that the lower cell area is due to differences in cell spreading on surfaces. This result suggested that enlazin may contribute to substrate adhesion. To test this, we used an adhesion assay that allows for overall adhesion of the cell population to be measured (Fey *et al*., 2002). In this assay, cells were rotated at specific speeds, beginning with 20 and increasing up to 200 rpm, and cells with adhesion defects detach at lower speeds than wild-type cells. Cells missing enlazin required less force to detach from the surface of the wells (Figure 4E). Thus, enlazin contributes to cell adhesion and cell spreading.

Table 2. Distribution of cytokinesis phenotypes

Strain	Cytokinesis phenotype (%)		
	Completed	Stalled/failed	n
wt(Ax3:Rep$^+$) control	98	2	64
wt(Ax3:Rep$^+$):*enlhp*	100	0	14
myoII:GFPtub, Hyg^R;control	100	0	19
myoII:GFPtub, Hyg^R;enlhp	60	40	45
myoII:GFPtub, Hyg^R;enl-tr	77	23	13
myoII:GFPcortI, Hyg^R;control	100	0	8
myoII:GFPcortI, Hyg^R;enlhp	67	33	6
myoII:GFPcortI, Hyg^R;enl-tr	64	36	11
myoII:GFPcortI, Hyg^R;myoII	100	0	4

Role of Enlazin in Cytokinesis

We examined cytokinesis of wt:enlhp cells by using time-lapse microscopy. Compared with controls, the *enlazin*-silenced cells seemed more rounded with less polar ruffling (Figure 4, F and G; Supplemental Movies 5 and 6). Interestingly, cells missing enlazin had altered bridge morphology, often failing to maintain a cylindrical bridge. Previously, we showed that wild-type cells form cylindrical bridges during phase 2 of cytokinesis (Zhang and Robinson, 2005). The *enlazin*-silenced cells seem to elongate normally, but during phase 2, the cylindrical bridge collapsed in about one-half of the cells, consistent with a defect in adhesion (Figure 4, F and G). We also silenced *enlazin* in "wild-type" (*myoII*$^-$:: GFPmyoII:pDRH, RFPα-tubulin:pDxA-Bl) cells to check the myosin-II distribution. Indeed, GFP-myosin-II localized normally to the cleavage furrow cortex in the absence of enlazin (Figure 4H). In this background, the enlhp cells again seemed more rounded during cytokinesis. Overall, in a wild-type background, silencing of *enlazin* did not increase the failure rate of cytokinesis on surfaces (Table 2).

Because the *myosin-II* mutant cells undergo cytokinesis by using a fundamentally different physical mechanism that requires surface-attachment, synthetic interactions with *myosin-II* can be particularly informative for discerning the function of a protein of interest (Nagasaki *et al*., 2002; Zhang and Robinson, 2005). Thus, we silenced *enlazin* in the *myosin-II* mutant background, creating *myoII*:enlhp cells (Figure 5A). We used time-lapse imaging to observe *myoII*:enlhp cells as they underwent cytokinesis. Using *myoII*:enlhp cells

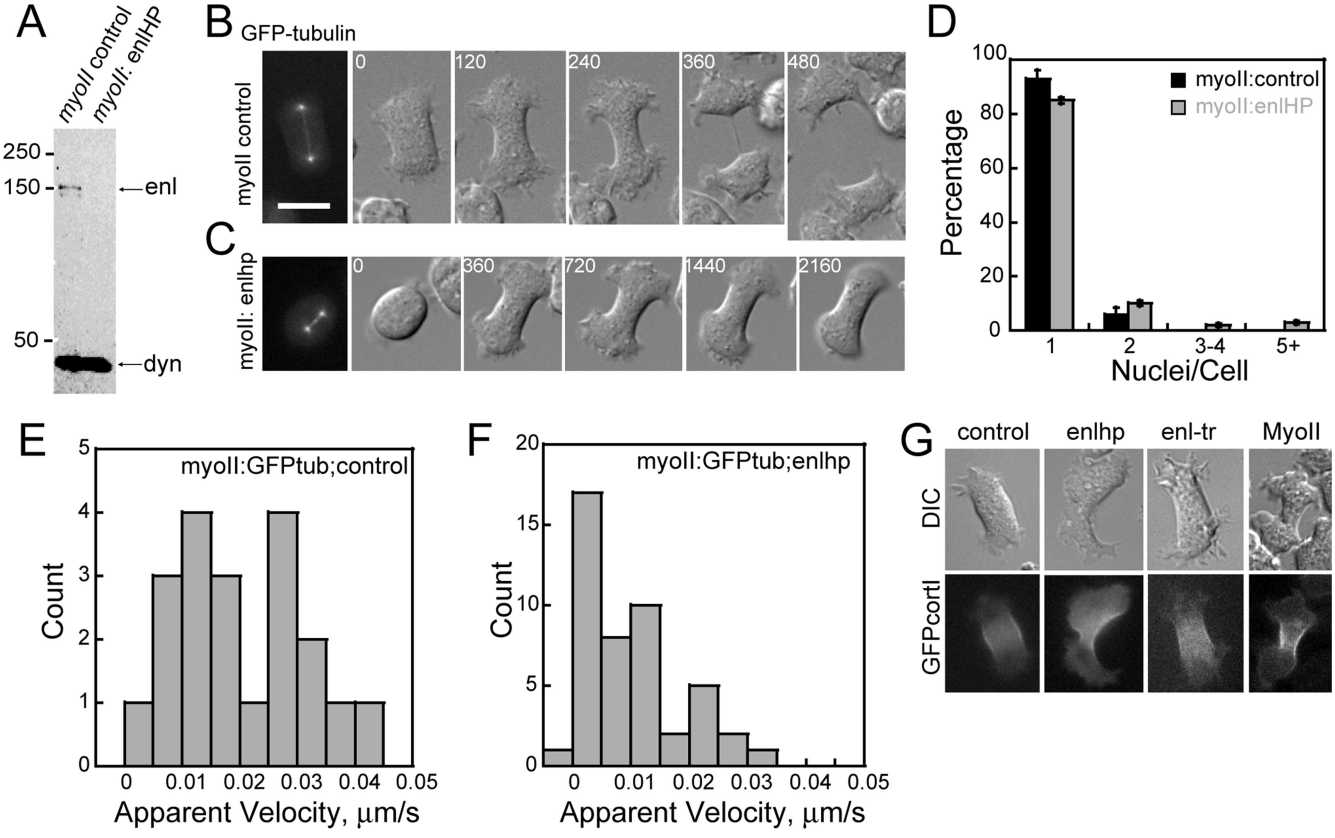

Figure 5. Enlazin is required for normal furrow ingression of *myoII* mutant cytokinesis. (A) Western analysis demonstrates that enlazin protein is depleted in *myoII*:enlhp cells. (B) Time series of *myoII*:GFP-α-tubulin, pDRH-HygR; pLD1A15SN control cells. (C) Time series of *myoII*:GFP-α-tubulin, pDRH-HygR; enlhp:pLD1 cells. The first panels in B and C show the anaphase spindles, demonstrating that the cells are mitotic. Bar in B, 10 μm and applies to B and C. (B and C) Time 0 is start of the movie. Time, seconds. (D) Histogram of nuclei/cell distributions for *myoII* control versus *myoII*:enlhp cells. Histograms derived from three samples per strain with 300–350 cells per sample. Error bars are SEMs. (E) Distribution of apparent furrow-thinning velocities for *myoII*::GFPtubulin:pDRH; pLD1A15SN (0.020 $\pm$ 0.0024 μm/s; mean $\pm$ SEM) cells. (F) Distribution of apparent furrow-thinning velocities for *myoII*::GFPtubulin:pDRH; enlhp (0.0094 $\pm$ 0.0013 μm/s; mean $\pm$ SEM) cells. The difference between these two distributions is significant (Student's *t* test, $p = 0.000393$). (G) GFP-cortexillin-I localizes to the cleavage furrows of *enlazin*-depleted *myoII* mutant cells. Cell background was *myoII*:GFPcortI, pDRH-Hyg^R and cells carry the pLD1A15SN vector (control), enlhp:pLD1, enl-tr:pLD1, or myosin-II:pBIG, which expresses untagged myosin-II heavy chain for a *wild-type* comparison.

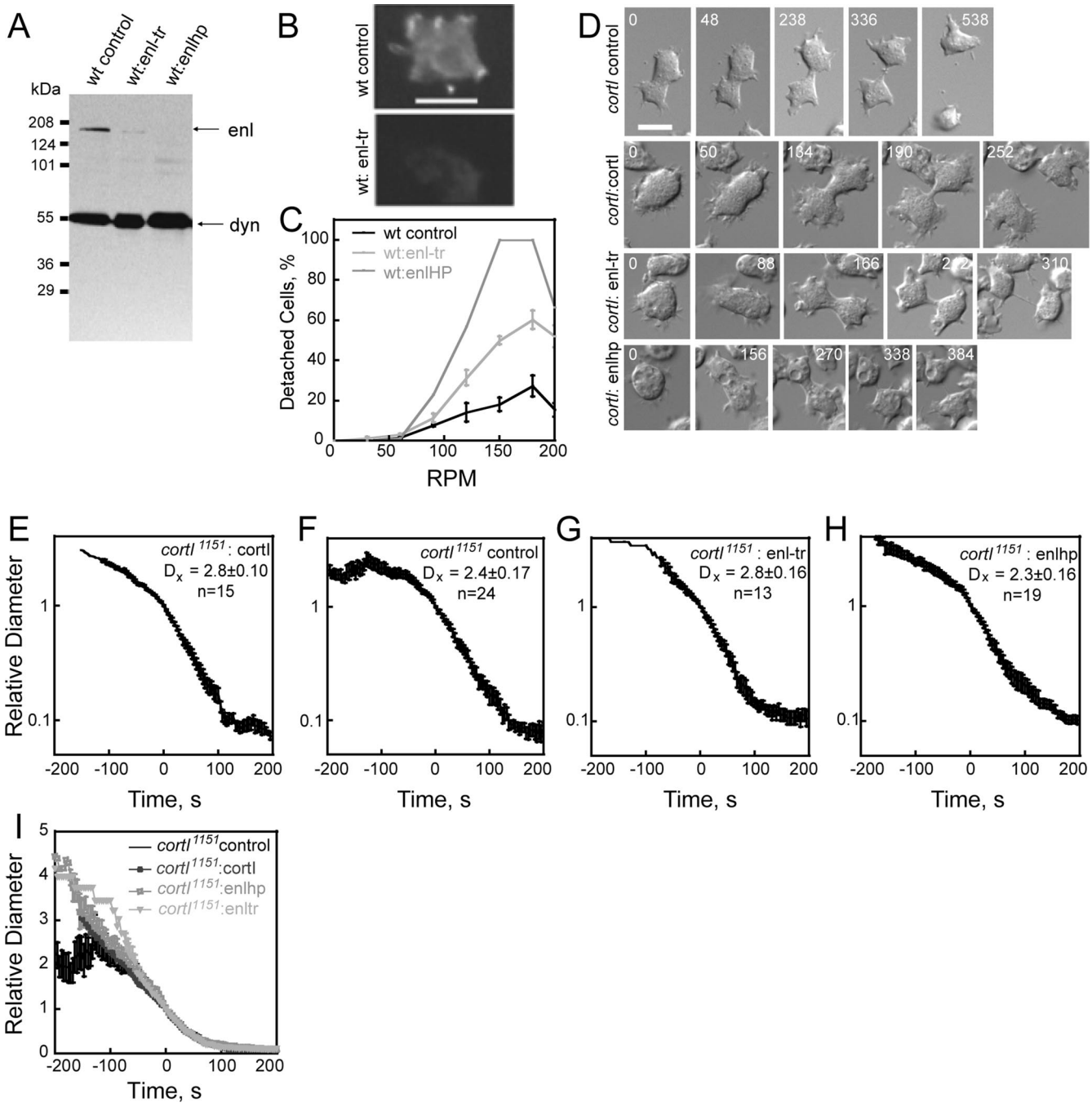

Figure 6. Enl-tr disrupts endogenous enlazin and removal of enlazin restores wild-type cytokinesis furrow-thinning dynamics to *cortexillin-I* cells. (A) Western analysis of cell extracts from wt control, wt:enl-tr, and wt:enlhp cells. Endogenous enlazin is significantly reduced in wt:enl-tr cells. Dynacortin is shown for comparison. (B) Immunocytochemistry of wild-type control cells (wt control image is repeated from Figure 3E for direct comparison) and wt:enl-tr cells. Bar, 10 μm. (C) Removal of enlazin by expression of enl-tr reduces the adhesion of wild-type cells. In this experiment, cells were seeded at a concentration of 3×10^5 cells/ml on six-well, nontissue culture treated plates and incubated overnight (~16 h). Samples were subjected to different rotational speeds for an hour. The fraction of detached cells was measured. Mean ± SEM of three replicas at each speed are plotted as a function of rpm. An iteration of wt:enlhp cells was included in this experiment for direct comparison. (D) Time series of DIC movies of *cortI*^{1151} control (carrying the empty vector), *cortI*^{1151}:cortI (complemented *cortexillin-I* mutant), *cortI*^{1151}:enltr and *cortI*^{1151}:enlhp cells. Time 0 is start of the movie. Time, seconds. Bar, 10 μm. (E–H) Rescaled furrow-thinning trajectories for each strain. The mean ± SEM of the D_x and the number of cells analyzed are presented in the graphs. Time 0 is the point that D_x was reached. The *cortI*^{1151}:cortI (E), *cortI*^{1151}:enltr (G) and *cortI*^{1151}:enlhp (H) cells had very similar furrow-thinning trajectories, whereas the *cortI*^{1151} control cells (F) were much slower in the −200 to −100-s time frame. I. Graph shows all four strains on the same linear–linear plot.

that also expressed GFP-α-tubulin, allowing the cells to be verified as mitotic, we observed that *myoII*:enlhp cells frequently arrested at the dumbbell stage for >30 min (compared with 6–8 min. typical of *myoII* control cells) and/or completely failed at cytokinesis as the furrow slipped toward one end (Figure 5, B versus C, and Supplemental

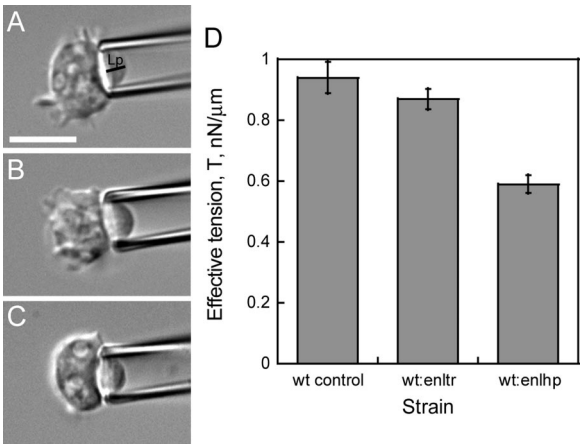

Figure 7. Micropipette aspiration reveals a role for enlazin in cortical resistance. (A–C) Micropipette aspiration of wt control (A), wt:enltr (B), and wt:enlhp (C) cells reveals mechanical differences. Pressures of 0.40 nN/μm^2 (A), 0.35 nN/μm^2 (B), and 0.25 nN/μm^2 (C) were applied until the tether length, L_p equaled the radius of the pipette, R_p. (D) Histogram of the effective tension of wt control, wt:enl-tr, and wt:enlhp cells. Data are mean ± SEM, n = 20 for each strain.

Movies 7 and 8). Overall, 40% of the *myoII*:GFP-α-tubulin; enlhp cells failed division compared with 0% of *myoII* control cells (Table 2). The *myoII*:enlhp cells also had a small increase in the number of multinucleated cells (Figure 5D); the relatively low incidence of multinucleated cells is consistent with the observed failure rate if there are other processes at work (see *Discussion*).

Because cells that stalled at the dumbbell stage might have completed at a much later time, we analyzed the apparent furrow-thinning velocities of *myoII* control and *myoII*:enlhp cells. This apparent velocity serves as an independent metric for comparing strains that does not require full knowledge of every cytokinetic outcome. The apparent velocity is defined as the distance traversed from the start to the end of the movie or up to the time that the furrow reached 0.2-μm diameter (the final bridge dwelling phase) divided by the time required to traverse this distance. By stopping at 0.2-μm diameter, we eliminate from the apparent velocity the final bridge breakup step, which is a separable process (Zhang and Robinson, 2005). The distributions of measured apparent velocities between the *myoII* control and *myoII*:enlhp cells were significantly different (Figure 5, E and F). Thus, overall *myoII*:enlhp furrows thin more slowly than the *myoII* control cells. The *myoII*:enlhp cells did localize GFP-cortexillin-I to the cleavage furrow cortex (Figure 5G and Table 2), ruling out a defect in recruiting cortexillin-I to the cleavage furrow cortex. We suggest that enlazin plays a role in *myosin-II* mutant cytokinesis dynamics by contributing to adhesion-dependent force-generation that is necessary for *myosin-II* mutants to divide on surfaces.

Enl-tr Disrupts Endogenous Enlazin

To analyze how enl-tr suppresses *cortI* mutant cells, we examined the expression of endogenous enlazin in cells expressing enl-tr. Surprisingly, endogenous enlazin expression was significantly knocked down (Figure 6A). By immunocytochemistry, endogenous enlazin was similarly undetectable in the presence of enl-tr (Figure 6B). By RNA analysis, endogenous *enlazin* mRNA was present at wild-type levels in cells expressing enl-tr, indicating that enl-tr does not have an RNA interference effect (data not shown). We also expressed a GFP-enl-tr, which failed to accumulate in cells but similarly disrupted endogenous enlazin expression (data not shown). Therefore, enl-tr seems to act as a dominant-negative mutant, possibly complexing with native enlazin or titrating a cofactor that is required for stability. However, expression of enl-tr is not identical to enlhp, because enl-tr increased the growth rate of wild-type and *cortI*^{1151} cells, whereas enlhp decreased the growth rate of these same cells (Table 1). This difference is probably due to the severity of the knockdown because enl-tr cells still express small amounts of enlazin, whereas enlhp cells do not.

Enl-tr acts as a hypomorphic loss-of-function *enlazin* mutant. Wild-type cells expressing enl-tr had an intermediate level of adhesion compared with wild-type control and wt:enlhp cells (Figure 6C). Similarly, *myoII*:enltr cells had an intermediate failure rate at cytokinesis (Table 2) while still recruiting GFP-cortexillin-I to the cleavage furrow cortex (Figure 5G). We then wondered whether enlhp and enl-tr could rescue cytokinesis dynamics of a *cortexillin-I* mutant. Although growth in suspension is a test of cytokinesis fidelity, other factors may influence the ability of cells to grow in suspension culture, because the cytoskeletal network is different between nonadherent and adherent cells (Gerald *et al*., 1998). Therefore, to rigorously and directly examine cytokinesis, we collected time-lapse DIC movies of *cortI*^{1151} mutant control (carrying an empty vector) cells, *cortI*^{1151} cells complemented with cortexillin-I, and *cortI*^{1151} mutant cells expressing either enl-tr or enlhp (Figure 6D and Supplemental Movies 9–12). The *cortI*^{1151} mutant cells displayed typical irregular morphology as observed previously (Weber *et al*., 2000; Girard *et al*., 2004), whereas *cortI*^{1151} cells expressing cortexillin-I, enl-tr, and enlhp displayed a much more symmetrical shape and formed a highly symmetrical bridge that ingressed evenly from both sides. Therefore, by morphological criteria, *cortI*^{1151} mutant cytokinesis could be rescued by complementation by cortexillin I or suppression by enlhp or enl-tr.

To quantify the cytokinesis dynamics of these cells, we analyzed the kinetics of furrow ingression for each strain by using our rescaling methods developed previously (see *Materials and Methods*) (Zhang and Robinson, 2005). The complemented *cortI*^{1151} mutant (*cortI*^{1151}:cortI) had the expected wild-type trajectory (Figure 6E), whereas the *cortI*^{1151} control cells had a slow phase 1 (from −200 to −100 s) (Figure 6F). Significantly, *cortI*^{1151} cells expressing either enl-tr or enlhp had nearly wild-type kinetics of furrow thinning (Figure 6, G and H). It is notable that all four strains were identical in their trajectories from −50 to 100 s, whereas differences between *cortI*^{1151}and the rescued strains occurred primarily from −200 to −100 s (Figure 6I). Thus, cortexillin-I seems to have its major role in furrow-thinning dynamics during the early stages of furrow ingression, and suppression of enlazin function quantitatively rescues this phase of *cortexillin-I* mutant cytokinesis.

Enlazin Contributes to Cell Cortex Mechanics

Because enlazin enriches in the cell cortex and contains a fimbrin domain, we hypothesized that enlazin may contribute to the mechanical resistance of the cortex. We used micropipette aspiration to measure the effective tension of wild-type cells and wild-type cells expressing enl-tr or enlhp (Figure 7). Expression of enl-tr, which partially reduced endogenous enlazin levels, caused a 7% reduction in cortical resistance compared with wild-type control; however, this difference is not statistically significant (Student's *t* test, p = 0.23). In contrast, a more complete inhibition of enlazin

expression by enlhp caused a significant 38% reduction in the effective cortical tension (Student's t test, $p < 0.0001$). This level of reduction in cortical resistance is similar to that observed in *cortexillin-I* mutants (Simson *et al.*, 1998; Girard *et al.*, 2004). Thus, enlazin contributes to cortical resistance.

DISCUSSION

Cytokinesis is a global cell shape change that requires the entire cytoskeletal network. Recent estimates place the number of proteins involved to be ≈200 (Eggert *et al.*, 2004; Skop *et al.*, 2004). Many proteins are expected to play important roles; however, given the robustness of the process, many of these proteins may not produce gross morphological defects when mutated. Thus, a conundrum is raised in that to probe the complexity and dynamics of cytokinesis, standard morphological genetic screens will fail to yield the majority of critical players. To circumvent this problem, interaction genetic approaches combined with quantitative analyses are required to identify relevant players.

Genetic Analysis of Global and Equatorial Pathways

Here, we have used interaction genetics to identify and characterize enlazin. Enlazin is a natural fusion of two classes of actin-associated proteins, the ERMs and fimbrin. ERMs link actin to membrane through the FERM domain, and fimbrin crosslinks actin filaments into bundles (Hirao *et al.*, 1996; Bretscher, 1999; Volkmann *et al.*, 2001). Thus, the current molecular model for enlazin is that it links actin filaments to the overlying plasma membrane. By connecting and integrating integral membrane adhesion proteins with the actin network, enlazin may form larger macromolecular cytoskeletal assemblies that simultaneously increase cortex resistance and cell–substrate adhesion.

Significantly, enlazin and dynacortin were discovered in the same genetic suppression experiment. Dynacortin, an actin filament bundling protein that functions in a global pathway for cytokinesis control, is required for normal cortical viscoelasticity and functions as a brake, slowing furrow ingression (Robinson and Spudich, 2000; Robinson *et al.*, 2002b; Girard *et al.*, 2004; Zhang and Robinson, 2005). Similarly, enlazin contains an actin-binding domain, is localized globally during cytokinesis, regulates cytokinesis furrow morphology and dynamics, and contributes to cortical resistance. Therefore, enlazin and dynacortin act in a global pathway that controls cytokinesis dynamics and cortex mechanics.

Enlazin Contributes to Cytokinesis Dynamics

Overall, enlazin contributes to two features of cytokinesis: adhesion and cortical mechanics. Each property has important roles in cytokinesis, and each becomes critical when the cytokinetic machinery is perturbed in specific ways such as by removing cortexillin-I or myosin-II. To begin unraveling the contributions of these properties to cytokinesis, we have been developing a quantitative framework for analyzing cytokinesis dynamics in the protozoan *Dictyostelium discoideum* (Robinson *et al.*, 2002a; Reichl *et al.*, 2005; Zhang and Robinson, 2005). In this framework, cytokinesis contractility is separable into three mechanical phases. Phase 1 is the movement away from an equilibrium position (the spherical mother cell) and requires energy input either through myosin-II mechanochemistry or adhesion-mediated traction forces. Phase 2 is a return to equilibrium (production of two spherical daughter cells), and during this phase, a cylindrical bridge is formed, which is predicted to be important for contributing additional forces (Laplace pressure), providing a boost for furrow thinning (Zhang and Robinson, 2005). Phase 3 is a bridge dwelling phase that requires cytoskeletal disassembly and cell separation.

Silencing of *enlazin* in wild-type cells demonstrates that enlazin is required for normal cytokinesis morphology, including maintenance of a cylindrical bridge during phase 2. By contributing to the mechanical resistance of the global actin network, enlazin may directly contribute to cell shape. However, given the recruitment of enlazin into cell surface structures and its role in adhesion, enlazin may also be involved in traction forces that lead to bridge formation.

Enlazin may contribute in several ways to the cytokinesis dynamics of *myosin-II* mutants, which are dependent on surface adhesion for cell division. By contributing to adhesion, enlazin may be needed to generate adhesive forces that allow *myosin-II* mutant cells to complete cytokinesis. These adhesive forces may become particularly important at the phase 1–2 transition, the stage when the *myoII*:enlhp cells become delayed (Zhang and Robinson, 2005). Alternatively, because enlazin contributes to cortical mechanics, its contribution to cortical resistance may be necessary to convert stresses generated from phase 1 cell elongation to (Laplace pressure-mediated) furrow-thinning of *myosin-II* mutants during phase 2 (Zhang and Robinson, 2005).

Silencing of *enlazin* in the *myosin-II* mutant background caused 40% of the division events to fail but surprisingly yielded a population consisting of <20% multinucleated cells. However, if other processes (such as different success/failure rates for division of multinucleated cells or cell death) affect the nuclei/cell distribution (essentially a multiprocess Markov chain), then this difference is not unexpected. For example, in a simple scenario, if mononucleated cells fail division 50% of the time, but binucleated cells successfully complete division producing four daughter cells 100% of the time, then a steady state of 80% mononucleated cells is quickly reached in an asynchronous culture. Thus, our data argue for the existence of other processes that affect the nuclei/cell distribution of the *myoII*:enlhp cells. For these reasons, bulk measurements of nuclei/cell distributions are insufficient and should not replace direct single cell analyses for discerning the contributions of proteins to cytokinesis dynamics.

In contrast to the *myosin-II* mutants, the *cortexillin-I* mutants have altered furrow morphology and slower dynamics during phase 1, and inhibition of enlazin corrects both defects. Because cortexillin-I contributes to cortex resistance and is enriched in the cleavage furrow cortex (Simson *et al.*, 1998; Weber *et al.*, 1999; Girard *et al.*, 2004), the mechanical integrity of the *cortexillin-I* furrow cortex must be altered. By removing globally distributed enlazin, the mechanical differential between the furrow and global cortices may be restored. It is worth pointing out that enl-tr rescued *cortexillin-I* cytokinesis with only small effects in cortical resistance as measured with the micropipette aspirator. This may be because enl-tr reduces enlazin levels enough to promote a more dynamic actin cortex without yielding a large effect on cortex resistance. Furthermore, micropipette aspiration works by deforming the cell, inducing strain on the cortex of the order of 5%. Thus, there can be nonlinear effects on cortex mechanics that mask a partial inhibition of enlazin. Because enl-tr suppressed growth-in-suspension defect of *cortexillin-I*, however, we suggest that its suppression is more reflective of the role of enlazin in cortex mechanics, remodeling, and deformability rather than its role in cell–substrate adhesion.

Cell Adhesion in Dictyostelium

Several proteins contribute to adhesion in *Dictyostelium*. Gp80 and ponticulin form the basis of a cell–cell adhesion system (Hitt *et al*., 1994; Harris *et al*., 2003), whereas filopodin (talin), an integrin β-like protein, and sadA are involved in cell–substrate adhesion (Simson *et al*., 1998; Fey *et al*., 2002; Cornillon *et al*., 2006). Significantly, enlazin, cortexillin-I, and filopodin (talin) have quantitative effects on both adhesion and cortical mechanics (Simson *et al*., 1998; Girard *et al*., 2004; this study). Actin-crosslinkers dynacortin and coronin also enrich in cell surface structures, suggesting that these proteins may similarly contribute in quantitative ways to adhesive forces (Robinson *et al*., 2002b). Thus, adhesion and cortex mechanics are controlled by a large number of overlapping cytoskeletal proteins. Genetic interactions of enlazin with *myoII* and *cortexillin-I* demonstrate how one protein can contribute to different cellular properties, each of which seems to become more significant in the context of other genetic lesions.

CONCLUSIONS

By combining interaction genetics with quantitative analyses of cytokinesis dynamics, we can identify the roles of proteins that contribute to the robustness and complexity of an essential shape change such as cytokinesis. Enlazin is an example of a protein that provides a critical function for cytokinesis dynamics but that would be missed in standard genetic screens for large multinucleated cells. Most gene products will likely prove to be factors that contribute to the more subtle dynamics of cellular processes rather than simply produce gross morphological defects when mutated. To access what will likely be a large fraction of the genome involved in regulating the shape changes of cytokinesis, the combination of interaction genetics and quantitative dynamics analyses are required to identify and discern the roles of these proteins.

ACKNOWLEDGMENTS

We thank the members of the Robinson laboratory for helpful discussions and comments on the manuscript. We thank Jan Faix for use of the Δ*cortI-214* cells and Jim Spudich for the use of the *myosin-II* mutant cells. E.O. was partially supported by a Postbaccalaureate Research Education Program Scholar award. We also thank the Burroughs-Wellcome Fund, the Beckman Foundation, the American Cancer Society (Grant IRG-58-005–41), and National Institutes of Health (R01 GM-066817) for support to D.N.R.

REFERENCES

Bretscher, A. (1999). Regulation of cortical structure by the ezrin-radixin-moesin protein family. Curr. Opin. Cell Biol. *11*, 109–116.

Cornillon, S., Gebbie, L., Benghezal, M., Nair, P., Keller, S., Wehrle-Haller, B., Charrette, S. J., Bruckert, F., Letourner, F., and Cosson, P. (2006). An adhesion molecule in free-living *Dictyostelium amoebae* with integrin β features. EMBO Rep. *7*, 617–621.

Daniels, M. J., Wang, Y., Lee, M., and Venkitaraman, A. R. (2004). Abnormal cytokinesis in cells deficient in the breast cancer susceptibility protein BRCA2. Science *306*, 876–879.

de Hostos, E. L., Rehfueβ, C., Bradtke, B., Waddell, D. R., Albrecht, R., Murphy, J., and Gerisch, G. (1993). *Dictyostelium* mutants lacking the cytoskeletal protein coronin are defective in cytokinesis and cell motility. J. Cell Biol. *120*, 163–173.

De Lozanne, A., and Spudich, J. A. (1987). Disruption of the *Dictyostelium* myosin heavy chain gene by homologous recombination. Science *236*, 1086–1091.

Derganc, J., Božic, B., Svetina, S., and Žekš, B. (2000). Stability analysis of micropipette aspiration of neutrophils. Biophys. J. *79*, 153–162.

Dey, P. (2004). Aneuploidy and malignancy: an unsolved equation. J. Clin. Pathol. *57*, 1245–1249.

Effler, J. C., Kee, Y.-S., Berk, J. M., Tran, M. N., Iglesias, P. A., and Robinson, D. N. (2006). Mitosis-specific mechanosensing and contractile protein redistribution control cell shape. Curr. Biol. *16*, 1962–1967.

Eggert, U. S., Kiger, A. A., Richter, C., Perlman, Z. E., Perrimon, N., Mitchison, T. J., and Field, C. M. (2004). Parallel chemical genetic and genome-wide RNAi screens identify cytokinesis inhibitors and targets. PLoS Biol. *2*, e379.

Evans, E., and Yeung, A. (1989). Apparent viscosity and cortical tension of blood granulocytes determined by micropipet aspiration. Biophys. J. *56*, 151–160.

Faix, J., Steinmetz, M., Boves, H., Kammerer, R. A., Lottspeich, F., Mintert, U., Murphy, J., Stock, A., Aebi, U., and Gerisch, G. (1996). Cortexillins, major determinants of cell shape and size, are actin-bundling proteins with a parallel coiled-coil tail. Cell *86*, 631–642.

Feinberg, A. P., and Vogelstein, B. (1983). A technique for radiolabeling DNA restriction endonuclease fragments to high specific activity. Anal. Biochem. *132*, 6–13.

Fey, P., Stephens, S., Titus, M. A., and Chisholm, R. L. (2002). SadA, a novel adhesion receptor in *Dictyostelium*. J. Cell Biol. *159*, 1109–1119.

Fujiwara, T., Bandi, M., Nitta, M., Ivanova, E. V., Bronson, R. T., and Pellman, D. (2005). Cytokinesis failure generating tetraploids promotes tumorigenesis in p53-null cells. Nature *437*, 1043–1047.

Gerald, N., Dai, J., Ting-Beall, H. P., and De Lozanne, A. (1998). A role for *Dictyostelium* racE in cortical tension and cleavage furrow progression. J. Cell Biol. *141*, 483–492.

Girard, K. D., Chaney, C., Delannoy, M., Kuo, S. C., and Robinson, D. N. (2004). Dynacortin contributes to cortical viscoelasticity and helps define the shape changes of cytokinesis. EMBO J. *23*, 1536–1546.

Girard, K. D., Kuo, S. C., and Robinson, D. N. (2006). *Dictyostelium* myosin-II mechanochemistry promotes active behavior of the cortex on long time-scales. Proc. Natl. Acad. Sci. USA *103*, 2103–2108.

Harris, T.J.C., Ravandi, A., Awrey, D. E., and Siu, C.-H. (2003). Cytoskeleton interactions involved in the assembly and function of glycoprotein-80 adhesion complexes in *Dictyostelium*. J. Biol. Chem. *278*, 2614–2623.

He, X., and Dembo, M. (1997). On the mechanics of the first cleavage division of the sea urchin egg. Exp. Cell Res. *233*, 252–273.

Hirao, M., Sato, N., Kondo, T., Yonemura, S., Monden, M., Sasaki, T., Takai, Y., Tsukita, S., and Tsukita, S. (1996). Regulation mechanism of ERM (ezrin/radixin/moesin) protein/plasma membrane association: possible involvement of phosphatidylinositol turnover and Rho-dependent signaling pathway. J. Cell Biol. *135*, 37–51.

Hitt, A. L., Hartwig, J. H., and Luna, E. J. (1994). Ponticulin is the major high affinity link between the plasma membrane and the cortical actin network in *Dictyostelium*. J. Cell Biol. *126*, 1433–1444.

Kanada, M., Nagasaki, A., and Uyeda, T. Q. (2005). Adhesion-dependent and contractile ring-independent equatorial furrowing during cytokinesis in mammalian cells. Mol. Biol. Cell *16*, 3865–3872.

Kurz, T., Pintard, L., Willis, J. H., Hamill, D. R., Gönczy, P., Peter, M., and Bowerman, B. (2002). Cytoskeletal regulation by the Nedd8 ubiquitin-like protein modification pathway. Science *295*, 1294–1298.

Matzke, R., Jacobson, K., and Radmacher, M. (2001). Direct, high-resolution measurement of furrow stiffening during division of adherent cells. Nat. Cell Biol. *3*, 607–610.

Nagasaki, A., de Hostos, E. L., and Uyeda, T.Q.P. (2002). Genetic and morphological evidence for two parallel pathways of cell-cycle-coupled cytokinesis in *Dictyostelium*. J. Cell Sci. *115*, 2241–2251.

O'Connell, C. B., Warner, A. K., and Wang, Y.-L. (2001). Distinct roles of the equatorial and polar cortices in the cleavage of adherent cells. Curr. Biol. *11*, 702–707.

Rappaport, R. (1996). Cytokinesis in Animal Cells, Cambridge, MA: Cambridge University Press.

Reichl, E. M., Effler, J. C., and Robinson, D. N. (2005). The stress and strain of cytokinesis. Trends Cell Biol. *15*, 200–206.

Robinson, D. N., Cavet, G., Warrick, H. M., and Spudich, J. A. (2002a). Quantitation of the distribution and flux of myosin-II during cytokinesis. BMC Cell Biol. *3*, 4.

Robinson, D. N., Ocon, S. S., Rock, R. S., and Spudich, J. A. (2002b). Dynacortin is a novel actin bundling protein that localizes to dynamic actin structures. J. Biol. Chem. *277*, 9088–9095.

Robinson, D. N., and Spudich, J. A. (2000). Dynacortin, a genetic link between equatorial contractility and global shape control discovered by library complementation of a *Dictyostelium discoideum* cytokinesis mutant. J. Cell Biol. *150*, 823–838.

Ruppel, K. M., Uyeda, T.Q.P., and Spudich, J. A. (1994). Role of highly conserved lysine 130 of myosin motor domain. In vivo and in vitro characterization of site specifically mutated myosin. J. Biol. Chem. *269*, 18773–18780.

Simson, R., Wallraff, E., Faix, J., Niewöhner, J., Gerisch, G., and Sackmann, E. (1998). Membrane bending modulus and adhesion energy of wild-type and mutant cells of *Dictyostelium* lacking talin or cortexillins. Biophys. J. *74*, 514–522.

Skop, A. R., Liu, H., Yates, J., Meyer, B. J., and Heald, R. (2004). Dissection of the mammalian midbody proteome reveals conserved cytokinesis mechanisms. Science *305*, 61–66.

Stukenberg, P. T. (2004). Triggering p53 after cytokinesis failure. J. Cell Biol. *165*, 607–608.

Volkmann, N., DeRosier, D., Matsudaira, P., and Hanein, D. (2001). An atomic model of actin filaments cross-linked by fimbrin and its implications for bundle assembly and function. J. Cell Biol. *153*, 947–956.

Weber, I., Gerisch, G., Heizer, C., Murphy, J., Badelt, K., Stock, A., Schwartz, J.-M., and Faix, J. (1999). Cytokinesis mediated through the recruitment of cortexillins into the cleavage furrow. EMBO J. *18*, 586–594.

Weber, I., Neujahr, R., Du, A., Köhler, J., Faix, J., and Gerisch, G. (2000). Two-step positioning of a cleavage furrow by cortexillin and myosin II. Curr. Biol. *10*, 501–506.

Zang, J.-H., Cavet, G., Sabry, J. H., Wagner, P., Moores, S. L., and Spudich, J. A. (1997). On the role of myosin-II in cytokinesis: division of *Dictyostelium* cells under adhesive and nonadhesive conditions. Mol. Biol. Cell *8*, 2617–2629.

Zhang, W., and Robinson, D. N. (2005). Balance of actively generated contractile and resistive forces controls cytokinesis dynamics. Proc. Natl. Acad. Sci. USA *102*, 7186–7191.

Zurek, B., Sanger, J. M., Sanger, J. W., and Jockusch, B. M. (1990). Differential effects of myosin-antibody complexes on contractile rings and circumferential belts in epitheloid cells. J. Cell Sci. *97*, 297–306.